P. Giguère
Graduate Research Assistant.
e-mail: giguere@uiuc.edu

M. S. Selig
Assistant Professor.
e-mail: m-selig@uiuc.edu

Department of Aeronautical and Astronautical Engineering,
University of Illinois at Urbana-Champaign,
306 Talbot Laboratory,
104 S. Wright Street,
Urbana, IL 61801-2935

New Airfoils for Small Horizontal Axis Wind Turbines

In a continuing effort to enhance the performance of small wind energy systems, one root airfoil and three primary airfoils were specifically designed for small horizontal axis wind turbines. These airfoils are intended primarily for 1–5 kW variable-speed wind turbines for both conventional (tapered/twisted) or pultruded blades. The four airfoils were wind-tunnel tested at Reynolds numbers between 100,000 and 500,000. Tests with simulated leading-edge roughness were also conducted. The results indicate that small variable-speed wind turbines should benefit from the use of the new airfoils which provide enhanced lift-to-drag ratio performance as compared with previously existing airfoils.

1 Introduction

Over the last 12 years, a considerable number of airfoils have been specifically developed for horizontal axis wind turbines (HAWTs). For example, 25 specially tailored airfoils for wind turbines originated from the joint work between the National Renewable Energy Laboratory (NREL) and Airfoils, Inc. (Tangler and Somers, 1995). For wind-turbine applications, the advanced NREL airfoils have been shown to provide aerodynamic and structural advantages as compared with airfoils originally designed for airplane applications. In addition, Björk (1988, 1989, 1990), Hill and Garrard (1989), Madsen and Rasmussen (1992), and Timmer and Rooy (1992) have also designed airfoils for HAWTs. There are, however, only a limited number of wind-turbine airfoils that have been developed exclusively for small blades.

Typically, the entire span of the blades of small HAWTs operate at low Reynolds numbers where laminar separation effects can severely degrade the performance of airfoils not designed for this flow regime. In addition, the typically fast rotational speeds of small HAWTs provide centrifugal stiffening that reduces the blade bending loads and thus, allows for the use of thinner airfoils as compared with those designed for larger wind turbines. Reductions in laminar separation effects and in airfoil thickness provide an increase in aerodynamic performance, which yields better energy capture. Therefore, owing to low Reynolds number aerodynamics and centrifugal stiffening effects, wind-turbine airfoils designed for medium and large blades are not particularly suitable for smaller blades.

A number of existing low Reynolds number airfoils, which were designed for small unmanned aerial vehicles, have been shown to be applicable to small wind turbines (Giguère and Selig, 1996, 1997a). Specially tailored airfoils for small HAWTs, however, should provide enhanced performance. From the literature, it appears that the S822 and S823 airfoils are the only two airfoils that have been specially designed for small blades. These two airfoils are principally intended for stall-regulated HAWTs and form one of the nine advanced NREL airfoil families (Tangler and Somers, 1995). Consequently, there is a need for new wind-turbine airfoils for small HAWTs, especially for those operating in variable-speed mode.

In a continuing effort to support new blade designs for small HAWTs and improve their performance, a total of four airfoils were designed and wind-tunnel tested. These airfoils are intended primarily for 1–5 kW rated power variable-speed wind turbines for conventional (tapered/twisted) or pultruded blades. Section 2 describes the airfoil design objectives and methodology. A brief description of the wind-tunnel facility, measurement techniques, and data reduction method is provided in Section 3. Section 4 provides a discussion of the wind-tunnel test results, including tests with fixed transition to simulate leading-edge roughness caused by blade erosion, accumulation of insect debris, etc. Finally, conclusions are given in Section 5.

2 Airfoil Design Objectives and Methodology

In this design work, the focus has been on designing airfoils that can be used along the entire blade span of small variable-speed HAWTs. Three airfoils, referred to as the primary airfoils, were designed to provide optimum performance over a broad range of operating conditions. Considering the low operating Reynolds numbers and beneficial centrifugal stiffening effects of small HAWTs, the airfoil thickness for the primary airfoils was fixed at ten percent. A 16 percent root airfoil was also designed to accommodate possible large root bending moment and large blade-stiffness requirements. With the root airfoil over the inboard 30 percent of the blade, the primary airfoils are recommended for use over the last 25 percent of the blade (from the 75 percent station to the tip), with blending between 30 percent and 75 percent of the blade span. The root airfoil (SG6040) and the three primary airfoils (SG6041, SG6042, and SG6043) are depicted in Fig. 1.

During normal operation, variable-speed HAWTs operate below stall and over a relatively limited lift range as compared with constant-speed wind turbines. For these operating conditions, minimizing leading-edge roughness effects, such as no loss in the maximum lift coefficient, is not particularly critical (Tangler and Somers, 1995; Tangler, 1997). For optimum aerodynamic performance during variable-speed operation, the low-drag lift range (drag bucket) can be reduced in favor of greater lift-to-drag ratios. Accordingly, the primary airfoils were designed to achieve as high a lift-to-drag ratio as possible at the design lift coefficient, ranging from 0.6 to 1.2. The primary airfoil having the lowest design lift coefficient was expected to yield large blade chords and consequently, the root airfoil was designed to be mainly used with the two other primary airfoils. To account for possible variations in the tip-speed ratio (TSR) caused by atmospheric turbulence, the best lift-to-drag conditions were designed to occur over a range of lift coefficients centered about the design lift coefficient.

The operational Reynolds number range for HAWTs having a rated power between 1–5 kW is typically below 1,000,000. At these Reynolds numbers and particularly below 500,000, minimizing laminar seperation effects is an important design driver. Accordingly, low design Reynolds numbers were favored to control laminar seperation effects. The design Reynolds numbers for the four airfoils were selected according to the

Contributed by the Solar Energy Division of THE AMERICAN SOCIETY OF MECHANICAL ENGINEERS for publication in the ASME JOURNAL OF SOLAR ENERGY ENGINEERING. Manuscript received by the ASME Solar Energy Division, July 1997; final revision, Dec. 1997. Associate Technical Editor: P. S. Veers.

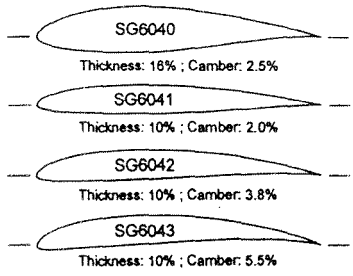

Fig. 1 Contours of the root and primary airfoils

Table 1 Airfoil design objectives

Airfoil	t/c	Design C_l	Design Re
SG6040	16%	1.1	200,000
SG6041	10%	0.6	500,000
SG6042	10%	0.9	333,333
SG6043	10%	1.2	250,000

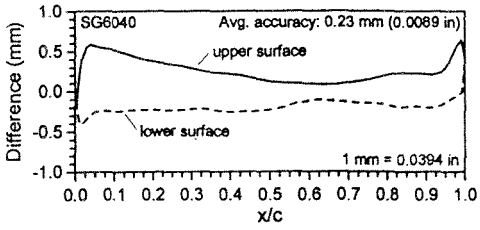

Fig. 2 Contour accuracy plot for the SG6040 airfoil

tradeoff between operating lift coefficient C_l and Reynolds number Re. It has been shown that for an optimum variable-speed rotor, the product of the lift coefficient and Reynolds number is nearly constant for a particular blade station (Giguère and Selig, 1997b), i.e.,

$$R = \mathrm{Re}\, C_l. \tag{1}$$

Here, R is the reduced Reynolds number which is constant so long as the TSR and the local velocity, which includes the axial induction factors, of a given blade station remain constant. Therefore, the potential increase in the maximum lift-to-drag ratio from operating at a high lift coefficient is reduced by a lower operating Reynolds number according to Eq. (1) and vice versa. The design Reynolds number for each primary airfoil was determined using Eq. (1) and a reduced Reynolds number R of 300,000. For the root airfoil, a design Reynolds number of 200,000 was used. The objectives for the four new airfoils are shown in Table 1.

To achieve the design objectives, the new airfoils were systematically designed using PROFOIL (Selig and Maughmer, 1992), which is an inverse airfoil design method. In addition, the Eppler code (Eppler, 1990) and XFOIL (Drela, 1989) were used to obtain preliminary airfoil performance characteristics to guide the design. With PROFOIL, the desired velocity distribution is prescribed, from which the corresponding airfoil shape is determined. In tailoring the velocity distribution for each airfoil, a gradual transition ramp was introduced on the upper surface to minimize laminar separation effects such as bubble drag. The need for a shallow pressure gradient combined with a high-lift requirement lead to aft-loading and, consequently, a relatively high pitching moment coefficient ($-0.08 < C_{m,c/4} < -0.14$). Note that the reduction in the size of the drag bucket caused by the use of aft-loading is not a drawback for variable-speed HAWTs because, as mentioned previously, they operate over a relatively limited lift range under normal operation. The primary airfoils have similar velocity distributions that differ mainly by their respective amount of aft-loading. Therefore, the aerodynamic characteristics of the three primary airfoils are related and these airfoils can be considered as an airfoil series. The addition of the root airfoil to the primary airfoils provides a unique airfoil family for variable-speed HAWTs.

3 Testing Apparatus and Methods

The experiments were performed in the University of Illinois at Urbana-Champaign low-turbulence subsonic wind tunnel having a 0.857 m (2.81 ft) high and 1.219 m (4 ft) wide test section. For the airfoil tests, two 1.829 m (6 ft) long Plexiglas splitter plates were inserted into the test section and reduced the test section width to 0.854 m (2.802 ft). With an empty test section, the turbulence intensity of the tunnel is less than 0.1 percent for the test Reynolds numbers (Guglielmo, 1996; Selig et al., 1995). The 0.305 m (1 ft) chord airfoil models were made of foam with a fiberglass finish and were inserted horizontally between the splitter plates with nominal gaps of 1–2 mm (0.040–0.080 in.). Using a coordinate measuring machine, each airfoil model was digitized at midspan. As an example of the digitized results, Fig. 2 presents the accuracy plot for the model of the SG6040 airfoil, which was the least accurate of the four models used in these tests. The average accuracy of the SG6040 airfoil model is, nevertheless, 0.23 mm (0.0089 in.) over the 305 mm (12 in.) chord. Similar plots for the primary airfoils can be found in Lyon et al. (1997a). The airfoil coordinates are tabulated in the Appendix.

The lift was directly measured using a strain-gage load cell, and the drag was determined from the average of four different span-

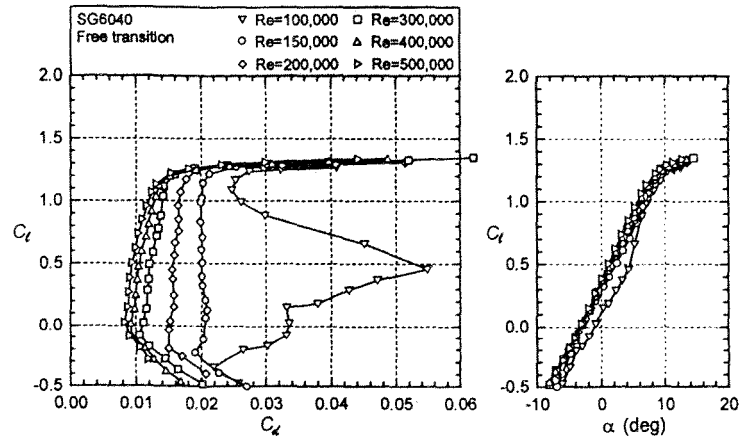

Fig. 3 Drag polars and corresponding lift curves for the SG6040 root airfoil (free transition)

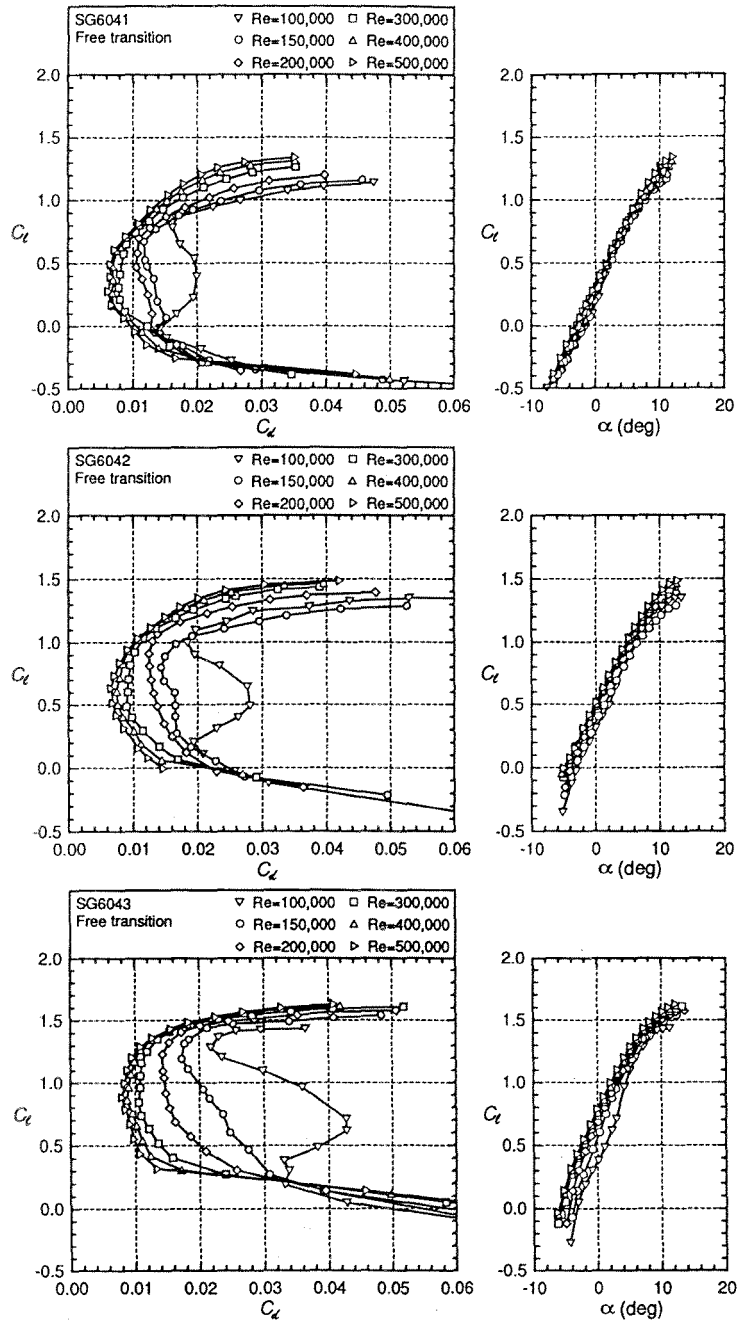

Fig. 4 Drag polars and corresponding lift curves for the SG6041, SG6042, SG6043 primary airfoils (free transition)

wise wake surveys spaced 76.2 mm (3 in.) apart (Selig et al., 1995; Lyon et al., 1997a). The overall uncertainty in both the lift and drag measurements was estimated to be 1.5 percent (Guglielmo, 1996; Selig et al., 1995; Lyon et al., 1997a). All measurements were corrected for wind-tunnel interference effects according to a method that has been validated with data from the NASA Langley Low Turbulence Pressure Tunnel (Giguère and Selig, 1997c; Lyon et al., 1997b). Finally, to simulate leading-edge roughness effects, a 0.58 mm (0.023 in.) zigzag trip was fixed to the upper and lower surface of the airfoils (Lyon et al., 1997a). In this paper, this trip size is referred to as the "standard" trip height. The trips were positioned in the vicinity of the suction peaks at two percent chord on the upper surface and at five percent chord on the lower surface. Note that transition does not occur immediately behind the trips but rather takes place over a finite distance (Lyon et al., 1997a). The use of trips instead of grit roughness elements has the advantage of being a more repeatable method, but the results obtained with the standard trips should be considered as a worst case scenario.

4 Wind Tunnel Test Results

This section provides an overview of the airfoil data obtained from the wind-tunnel tests conducted with the four new airfoils. The complete data set for a Reynolds number range of 100,000–500,000 can be found in Lyon et al. (1997a). Even though this Reynolds number range might not covers the entire operational range of small 1–5 kW HAWTs, data above a Reynolds number of 500,000 can generally be obtained quite accurately from logarithmic and linear extrapolation for the drag and lift, respectively. The drag variations are largest below a Reynolds number of 300,000 and thus, data in that range is more critical to document for small wind turbines.

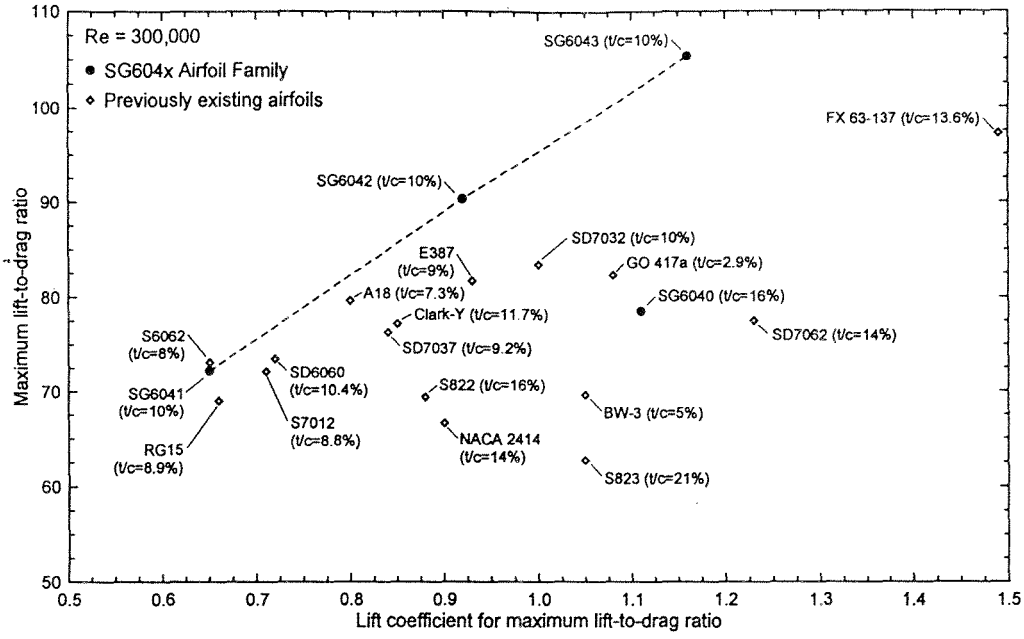

Fig. 5 Maximum lift-to-drag ratio versus the corresponding lift coefficient of various airfoils for small HAWTs (Re = 300,000)

Tests with free transition (no trips applied to the airfoil) were conducted at six Reynolds numbers from 100,000 to 500,000. Figures 3 and 4 present the drag polars and corresponding lift curves for the root and primary airfoils, respectively. These figures show that the design objectives have been met. For example, the maximum lift-to-drag ratio of the SG6042 occurs near a lift coefficient of 0.9 at its design Reynolds number and also over most of the Reynolds number range considered. Furthermore, the objective of providing a range of lift coefficients for which best lift-to-drag ratio performance occurs has also been satisfied. Therefore, performance penalties owing to off-design conditions should be relatively small except for a Reynolds number of 100,000 where laminar separation effects caused a large increase in drag. It should be emphasized, however, that such performance at a Reynolds number of 100,000 is typical of most low Reynolds airfoils (Giguère and Selig, 1996; Selig et al., 1995).

Figure 5 indicates the maximum lift-to-drag ratio and corresponding lift coefficient under clean conditions of the SG604x airfoil family and other low Reynolds number airfoils applicable to small HAWTs. The results are shown for a Reynolds number of 300,000, which is representative of the data for other Reynolds numbers, and the thickness of each airfoil is also shown. Note that all the data shown in Fig. 5 is based on wind tunnel experiments conducted with the testing apparatus and methods described in Section 3. As indicated in Fig. 5, the new airfoils provide lift-to-drag ratios that are equivalent or exceeding those of previously existing low Reynolds airfoils over a wide range of design lift coefficients. Therefore, small variable-speed HAWTs are likely to benefit from enhanced energy capture from the use of the new airfoils. Note, however, that comparing data for constant Reynolds number can be misleading based on the previously mentioned tradeoff between operating lift coefficient and Reynolds number. A better figure of merit to use in comparing the airfoils would be the maximum lift-to-drag ratio for a given reduced Reynolds number (Giguère and Selig, 1997a). Nonetheless, the results shown in Fig. 5 are indicative of the potential of the new airfoils for small variable-speed wind turbines.

For the tests with "fixed" transition, three Reynolds numbers were considered for each airfoil: 150,000, 300,000, and 500,000. An overview of these results is shown in Fig. 6 with results for a Reynolds number of 300,000. To facilitate comparison, the drag polar of each airfoil is shown for both free and

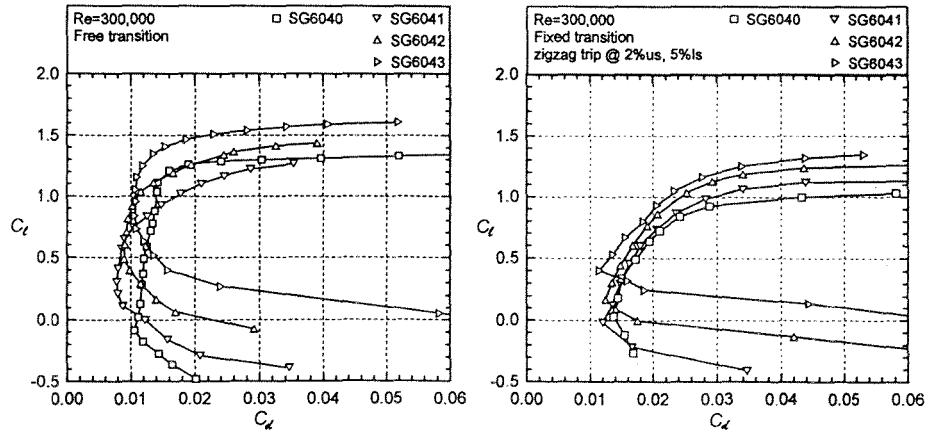

Fig. 6 Drag polars for the root and the primary airfoils at a Reynolds number of 300,000 (free and fixed transition)

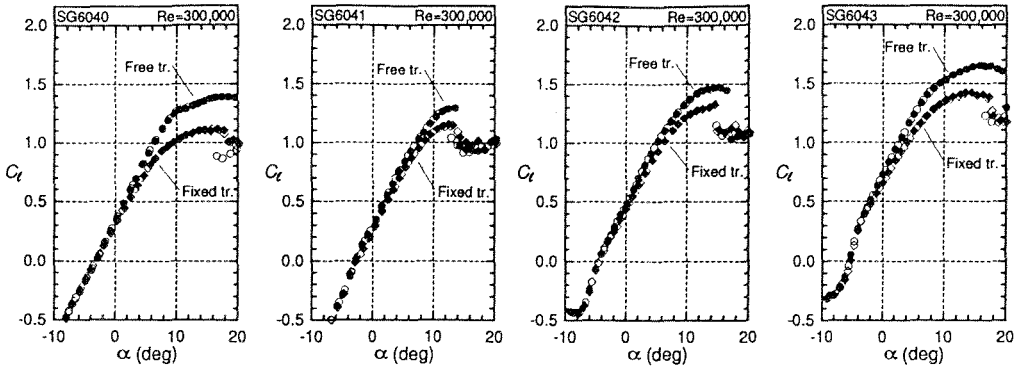

Fig. 7 Lift curves for the root and the primary airfoils at their design Reynolds numbers (free and fixed transition): dark symbols, increasing α and open symbols, decreasing α

fixed transition. In these tests, the standard trip as defined in Section 3 was used. As expected, the higher the design lift coefficient and relative thickness of the airfoil, the higher is the loss in performance caused by forcing transition. Furthermore, the lift coefficient corresponding to the maximum lift-to-drag ratio is also influenced by the simulated roughness at the leading edge. The change in lift coefficient for maximum lift-to-drag ratio can be explained by the results presented in Fig. 7. Even though the lift coefficients for maximum lift-to-drag ratio vary between the free and fixed transition cases (Fig. 6), it can be seen from Fig. 7 that the angle of attack for which maximum lift-to-drag ratio occurs remains, however, relatively constant. For example, Fig. 6 indicates that the lift coefficient for maximum lift-to-drag ratio of the SG6043 airfoil with free and fixed transition is 1.16 and 0.93, respectively. The lift curves for the SG6043 airfoil shown in Fig. 7 indicates that these lift coefficients correspond to an angle of attack of 4 deg. Therefore, a blade designed with the new airfoils should yield optimum performance even with leading-edge roughness. Based on the loss in maximum lift coefficient shown in Fig. 7, the use of the new airfoils should not be extended to small stall-regulated HAWTs. Airfoils such as the NREL S822 and S823 are better candidates in that case. The new airfoils, due largely to lower thickness, provide much better lift-to-drag ratio performance as compared with the S822 and S823 airfoils.

Table 2 summarizes the maximum lift coefficient, maximum lift-to-drag ratio and the corresponding lift coefficient for both the free and fixed transition cases of the SG604x airfoil family. As expected, the results presented in Table 2 indicate that the sensitivity to roughness of the airfoil performance increases with the design lift coefficient (Tangler, 1997). Note, however, that for a given Reynolds number, the maximum lift-to-drag ratios with fixed transition of the airfoil having the highest design lift coefficient (SG6043) remain the largest of all the new airfoils. In addition, the lift-to-drag ratio characteristics of the airfoils with fixed transition are for the most part independent of the Reynolds number. Consequently, blades using the SG6043 airfoil are likely to yield the best energy capture in the presence of leading-edge roughness elements. Such blades, however, are also likely to be most affected by Reynolds number effects owing to the high design lift coefficient of the SG6043 airfoil.

Table 2 Performance summary for the SG604x airfoil family

	SG6040 (root airfoil)						SG6041 (primary airfoil)					
	Free transition			Fixed transition			Free transition			Fixed transition		
Re	$C_{l_{max}}$	C_l ; $(l/d)_{max}$	$(l/d)_{max}$	$C_{l_{max}}$	C_l ; $(l/d)_{max}$	$(l/d)_{max}$	$C_{l_{max}}$	C_l ; $(l/d)_{max}$	$(l/d)_{max}$	$C_{l_{max}}$	C_l ; $(l/d)_{max}$	$(l/d)_{max}$
100,000	1.29	1.16	46.0	1.08	-	-	1.15	0.86	51.5	1.08	-	-
150,000	1.33	1.21	57.0	1.09	0.70	33.1	1.16	0.67	57.5	1.09	0.80	33.3
200,000	1.35	1.17	66.3	1.09	-	-	1.22	0.70	64.1	1.14	-	-
300,000	1.39	1.11	78.5	1.11	0.84	34.7	1.29	0.65	72.2	1.16	0.87	36.7
400,000	1.42	1.13	83.5	1.13	-	-	1.34	0.60	80.0	1.19	-	-
500,000	1.42	1.13	86.6	1.14	0.76	36.7	1.36	0.61	84.4	1.20	0.77	39.4
	SG6042 (primary airfoil)						SG6043 (primary airfoil)					
	Free transition			Fixed transition			Free transition			Fixed transition		
Re	$C_{l_{max}}$	C_l ; $(l/d)_{max}$	$(l/d)_{max}$	$C_{l_{max}}$	C_l ; $(l/d)_{max}$	$(l/d)_{max}$	$C_{l_{max}}$	C_l ; $(l/d)_{max}$	$(l/d)_{max}$	$C_{l_{max}}$	C_l ; $(l/d)_{max}$	$(l/d)_{max}$
100,000	1.35	1.10	55.6	1.26	-	-	1.52	1.37	59.4	1.36	-	-
150,000	1.29	0.89	59.7	1.27	0.83	38.7	1.56	1.31	74.2	1.38	1.01	42.0
200,000	1.41	1.01	77.8	1.28	-	-	1.59	1.33	86.6	1.40	-	-
300,000	1.47	0.92	90.3	1.32	0.86	41.5	1.65	1.16	105.3	1.42	0.93	45.2
400,000	1.50	0.93	101.0	1.33	-	-	1.68	1.17	118.0	1.44	-	-
500,000	1.52	0.84	105.9	1.34	0.90	45.7	1.70	1.10-1.20	125.1	1.43	0.98	48.4

The data shown so far with fixed transition has been for a fixed trip height, namely the standard trip. The effect of reducing the height of the trip was also investigated, and the results for the SG6042 airfoil at a Reynolds number of 300,000 are shown in Fig. 8. A total of five different zigzag trip heights were used ranging from 0.13 mm (0.005 in.) or 0.04 percent chord to 0.56 mm (0.023 in.—standard trip) or 0.19 percent chord. The results indicate that trips thicker than the smallest one caused a rapid degradation in airfoil performance.

Further tests were performed with plain trips to investigate whether or not the new airfoils were optimized for low drag at their respective design points. The tradeoff to consider involves reducing bubble drag at the cost of increased device drag—drag caused by the trip itself. For the SG6042 airfoil, a 0.15 mm (0.006 in.) thick plain (tape type) trip was positioned at different chordwise positions on the upper surface at the respective design lift coefficient. The results shown in Fig. 9 clearly indicate that the addition of the plain trip did not lead to any drag reduction beyond the experimental uncertainty of the measurements. In addition, three additional plain trip heights were also tested at 35 percent chord and the same Reynolds number of 300,000. As indicated in Fig. 10, trips thicker than the baseline (0.15 mm) were not beneficial in reducing the overall drag. Similar results were also obtained for the SG6043 airfoil at Reynolds numbers of 200,000 and 300,000. Therefore, the airfoils do have low bubble drag that likely cannot be reduced through the use of a trip or turbulator. Finally, the four airfoils considered as a group provide excellent lift-to-drag ratios over a broad range of lift conditions and are well suited for their intended application.

5 Conclusions

The airfoils designed during this work form a unique airfoil family for small variable-speed HAWTs. Wind-tunnel tests of the root airfoil (SG6040) and three primary airfoils (SG6041, SG6042, and SG6043) provided an extensive airfoil data set that can be used in the design of small blades. The two primary airfoils having the highest design lift coefficients (SG6042 and SG6043) yielded enhanced lift-to-drag performance over many other low Reynolds number airfoils. Consequently, small variable-speed wind turbines are likely to benefit from the use of these two airfoils. The SG6040 root airfoil and low-lift SG6041 airfoil are also likely to enhance the energy capture of small variable-speed HAWTs owing to structural requirements and

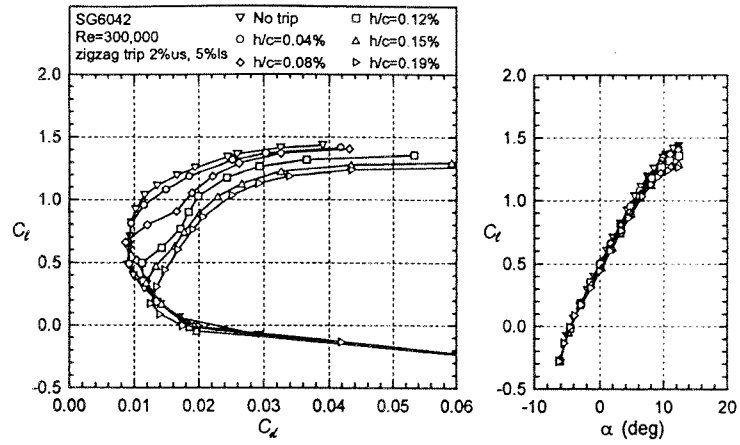

Fig. 8 Drag polars and corresponding lift curves for the SG6042 airfoil with varying zigzag trip heights

the tradeoff between operating lift coefficient and Reynolds numbers. Overall, the new airfoils provide excellent lift-to-drag ratios over a broad range of lift conditions and are well suited for small variable-speed wind turbines.

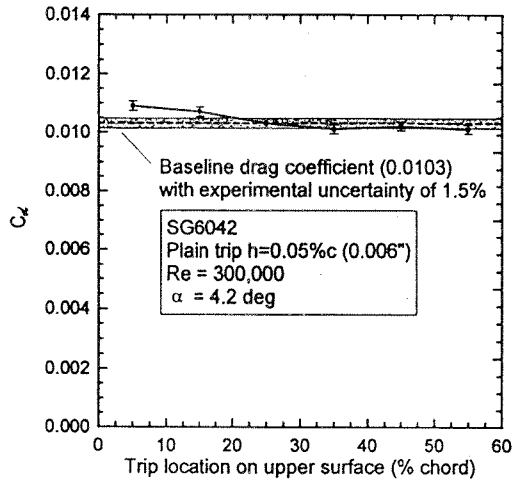

Fig. 9 Drag coefficient as a function of the chordwise position of a *h/c* = 0.05 percent plain trip on the upper surface

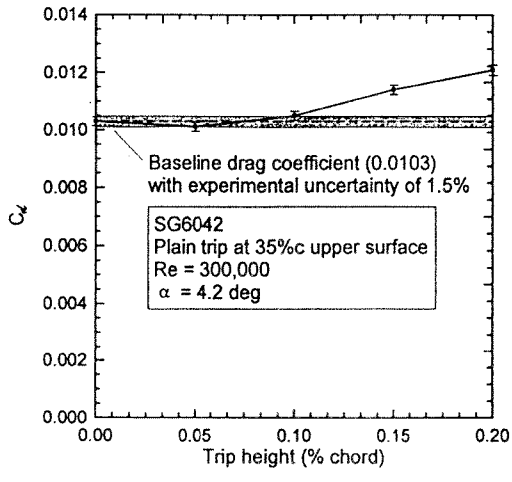

Fig. 10 Drag coefficient as a function of the normalized height of a plain trip positioned at 35 percent chord on the upper surface

Acknowledgments

The support from the National Renewable Energy Laboratory under subcontract XAF-4-14076-03 is gratefully acknowledged. Also, the authors would like to thank James L. Tangler of NREL for many useful discussions throughout this work. Finally, the authors are also thankful to Mark Allen of Allen Developments for building the four wind-tunnel models used in this study.

References

Björk, A., 1988, "Airfoil Design for Horizontal Axis Wind Turbines," *Proceedings of the Second IEA Symposium on Joint Action on Aerodynamics of Wind Turbines,* Lyngby, Nov., pp. 204–230.

Björk, A., 1989, "Airfoil Design for Variable RPM Horizontal Axis Wind Turbines," *Proceedings EWEC 89, European Wind Energy Conference,* Glasgow, Scotland.

Björk, A., 1990, "Coordinates and Calculation for the FFA-W1-xxx, FFA-W2-xxx, FFA-W3-xxx Series of Airfoils for Horizontal Axis Wind Turbines," The Aeronautical Research Institute of Sweden, Technical Report, FFA TN 1990-15.

Drela, M., 1989, "XFOIL: An Analysis and Design System for Low Reynolds Number Airfoils," *Lecture Notes in Engineering: Low Reynolds Number Aerodynamics,* T. J. Mueller, ed., Vol. 54, Springer-Verlag, New York, June.

Eppler, R., 1990, *Airfoil Design and Data,* Springer-Verlag, New York.

Giguère, P., and Selig, M. S., 1996, "Aerodynamic Performance of Small Wind Turbines Operating at Low Reynolds Numbers," American Wind Energy Association WIND POWER '96 Conference, June 23–27, Denver, CO.

Giguère, P., and Selig, M. S., 1997a, "Low Reynolds Number Airfoils for Small Horizontal Axis Wind Turbines," *Wind Engineering, 1997,* Vol. 21, No. 6, 1997.

Giguère, P., and Selig, M. S., 1997b, "Desirable Airfoil Characteristics for Large Variable-Speed Horizontal Axis Wind Turbines," ASME JOURNAL OF SOLAR ENERGY ENGINEERING, Vol. 119, August, pp. 253–260.

Giguère P., and Selig, M. S., 1997c, "Velocity Correction for Two Dimensional Tests with Splitter Plates," *AIAA J.,* Vol. 35, No. 7, pp. 1195–1200.

Guglielmo, J., 1996, "Spanwise Drag Variations at Low Reynolds Numbers," Department of Aeronautical and Astronautical Engineering Department, University of Illinois at Urbana-Champaign, Urbana, IL, May.

Hill, G. C., and Garrard, A. D., 1989, "Design of Aerofoils for Wind Turbine Use," *Proceedings of the European Wind Energy Conference,* Glasgow, Scotland.

Lyon, C. A., Broeren, A. P., Giguère, P., Gopalarathnam, A., and Selig, M. S., 1997a, *Summary of Low-Speed Airfoil Data—Volume 3,* SoarTech Publications, 1504 N, Horseshoe Circle, Virginia Beach, VA.

Lyon, C. A., Selig, M. S., and Broeren, A. P., 1997b, "Boundary-Layer Trips on Airfoils at Low Reynolds Numbers," AIAA Paper 97-0511.

Madsen, H. A., and Rasmussen, F., 1992, "Experiences in Airfoil Analysis and Design," *Proceedings of the Sixth IEA Symposium on the Aerodynamics of Wind Turbines,* Petten, Netherlands.

Selig, M. S., and Maughmer, M. D., 1992, "Generalized Multipoint Inverse Airfoil Design," *AIAA J.,* Vol. 30, No. 11, pp. 2618–2625.

Selig, M. S., Guglielmo, J. J., Broeren, A. P., and Giguère, P., 1995, *Summary of Low-Speed Airfoil Data—Volume 1,* SoarTech Publications, 1504 N, Horseshoe Circle, Virginia Beach, VA.

Tangler, J. L., and Somers, D. M., 1995, "NREL Airfoil Families for HAWTs," American Wind Energy Association WINDPOWER'95 Conference, May 9–12, Washington, DC.

Tangler, J. L., 1997, "Influence of Pitch, Twist and Taper on a Blade's Performance Loss Due to Roughness," ASME JOURNAL OF SOLAR ENERGY ENGINEERING, Vol. 119, pp. 248–252.

Timmer, W. A., and Rooy, R. P. J. O. M. van, 1992, "Thick Airfoils for HAWTs," *J. of Wind Engineering and Industrial Aerodynamics,* Vol. 39, May.

APPENDIX: Airfoil Coordinates

SG6040	
x/c	y/c
1.00000	0.00000
0.99788	0.00048
0.99183	0.00207
0.98233	0.00477
0.96977	0.00845
0.95442	0.01283
0.93637	0.01766
0.91559	0.02285
0.89221	0.02845
0.86647	0.03446
0.83861	0.04080
0.80887	0.04739
0.77752	0.05415
0.74482	0.06094
0.71104	0.06759
0.67632	0.07394
0.64081	0.07992
0.60477	0.08541
0.56837	0.09032
0.53180	0.09461
0.49526	0.09815
0.45891	0.10089
0.42297	0.10279
0.38758	0.10378
0.35286	0.10386
0.31903	0.10299
0.28619	0.10116
0.25449	0.09843
0.22405	0.09479
0.19496	0.09028
0.16734	0.08506
0.14137	0.07921
0.11719	0.07283
0.09496	0.06598
0.07481	0.05875
0.05686	0.05123
0.04123	0.04347
0.02798	0.03559
0.01725	0.02771
0.00913	0.01987
0.00362	0.01212
0.00072	0.00449
0.00027	-0.00268
0.00289	-0.00884
0.00906	-0.01450
0.01829	-0.02023
0.03027	-0.02580
0.04483	-0.03103
0.06202	-0.03566
0.08193	-0.03971
0.10446	-0.04336
0.12939	-0.04657
0.15655	-0.04937
0.18574	-0.05172
0.21677	-0.05361
0.24943	-0.05503
0.28349	-0.05594
0.31873	-0.05632
0.35490	-0.05613
0.39177	-0.05528
0.42916	-0.05371
0.46691	-0.05132
0.50479	-0.04801
0.54298	-0.04368
0.58164	-0.03863
0.62049	-0.03323
0.65925	-0.02772
0.69762	-0.02231
0.73526	-0.01718
0.77181	-0.01250
0.80690	-0.00840
0.84016	-0.00497
0.87120	-0.00228
0.89963	-0.00033
0.92511	0.00090
0.94728	0.00148
0.96587	0.00154
0.98063	0.00122
0.99132	0.00070
0.99782	0.00022
1.00000	0.00000

SG6041	
x/c	y/c
1.00000	0.00000
0.99801	0.00029
0.99227	0.00132
0.98311	0.00310
0.97084	0.00560
0.95568	0.00867
0.93778	0.01217
0.91722	0.01600
0.89412	0.02018
0.86872	0.02469
0.84127	0.02946
0.81200	0.03438
0.78119	0.03933
0.74901	0.04408
0.71552	0.04849
0.68087	0.05261
0.64526	0.05635
0.60884	0.05967
0.57186	0.06258
0.53448	0.06502
0.49692	0.06699
0.45939	0.06847
0.42211	0.06944
0.38529	0.06991
0.34915	0.06987
0.31389	0.06931
0.27971	0.06824
0.24683	0.06666
0.21540	0.06458
0.18563	0.06201
0.15767	0.05896
0.13169	0.05546
0.10783	0.05149
0.08618	0.04710
0.06690	0.04231
0.05002	0.03711
0.03555	0.03159
0.02361	0.02578
0.01411	0.01971
0.00702	0.01366
0.00241	0.00767
0.00016	0.00194
0.00029	-0.00270
0.00378	-0.00645
0.01080	-0.01010
0.02073	-0.01346
0.03361	-0.01637
0.04948	-0.01888
0.06829	-0.02104
0.08990	-0.02294
0.11413	-0.02461
0.14081	-0.02605
0.16976	-0.02728
0.20077	-0.02828
0.23363	-0.02907
0.26812	-0.02964
0.30402	-0.02998
0.34108	-0.03010
0.37907	-0.02997
0.41772	-0.02959
0.45679	-0.02894
0.49604	-0.02797
0.53524	-0.02663
0.57423	-0.02493
0.61284	-0.02285
0.65090	-0.02037
0.68832	-0.01763
0.72492	-0.01482
0.76041	-0.01210
0.79448	-0.00956
0.82683	-0.00728
0.85718	-0.00532
0.88524	-0.00370
0.91073	-0.00243
0.93339	-0.00149
0.95300	-0.00083
0.96938	-0.00036
0.98244	-0.00005
0.99204	0.00008
0.99798	0.00006
1.00000	0.00000

SG6042	
x/c	y/c
1.00000	0.00000
0.99806	0.00048
0.99249	0.00203
0.98372	0.00463
0.97210	0.00811
0.95784	0.01223
0.94102	0.01672
0.92161	0.02148
0.89968	0.02657
0.87546	0.03195
0.84915	0.03756
0.82098	0.04333
0.79117	0.04914
0.75995	0.05489
0.72757	0.06038
0.69410	0.06544
0.65962	0.07006
0.62435	0.07417
0.58844	0.07772
0.55208	0.08071
0.51546	0.08310
0.47877	0.08486
0.44221	0.08600
0.40597	0.08648
0.37024	0.08634
0.33522	0.08556
0.30110	0.08415
0.26808	0.08215
0.23633	0.07956
0.20603	0.07639
0.17735	0.07269
0.15044	0.06847
0.12544	0.06379
0.10249	0.05866
0.08169	0.05313
0.06316	0.04726
0.04698	0.04105
0.03315	0.03458
0.02179	0.02795
0.01284	0.02119
0.00619	0.01446
0.00197	0.00797
0.00011	0.00182
0.00035	-0.00341
0.00371	-0.00730
0.01068	-0.01042
0.02068	-0.01311
0.03369	-0.01516
0.04982	-0.01659
0.06901	-0.01751
0.09117	-0.01805
0.11611	-0.01826
0.14365	-0.01821
0.17358	-0.01792
0.20570	-0.01744
0.23979	-0.01679
0.27559	-0.01599
0.31286	-0.01506
0.35135	-0.01401
0.39078	-0.01286
0.43089	-0.01159
0.47140	-0.01016
0.51208	-0.00853
0.55277	-0.00671
0.59330	-0.00475
0.63345	-0.00273
0.67298	-0.00077
0.71161	0.00102
0.74904	0.00255
0.78494	0.00377
0.81900	0.00462
0.85093	0.00510
0.88041	0.00521
0.90718	0.00496
0.93097	0.00442
0.95153	0.00364
0.96868	0.00273
0.98224	0.00178
0.99204	0.00090
0.99800	0.00026
1.00000	0.00000

SG6043	
x/c	y/c
1.00000	0.00000
0.99811	0.00066
0.99274	0.00271
0.98439	0.00607
0.97343	0.01047
0.96007	0.01552
0.94429	0.02092
0.92597	0.02655
0.90516	0.03248
0.88207	0.03868
0.85688	0.04510
0.82979	0.05165
0.80101	0.05824
0.77074	0.06478
0.73922	0.07114
0.70666	0.07717
0.67320	0.08268
0.63889	0.08761
0.60396	0.09190
0.56854	0.09551
0.53276	0.09842
0.49685	0.10059
0.46096	0.10201
0.42528	0.10269
0.39000	0.10260
0.35527	0.10175
0.32131	0.10017
0.28827	0.09788
0.25633	0.09491
0.22567	0.09127
0.19645	0.08702
0.16882	0.08220
0.14293	0.07684
0.11890	0.07100
0.09687	0.06473
0.07694	0.05809
0.05920	0.05117
0.04376	0.04398
0.03062	0.03659
0.01983	0.02916
0.01142	0.02171
0.00528	0.01436
0.00150	0.00741
0.00002	0.00094
0.00059	-0.00468
0.00393	-0.00860
0.01077	-0.01120
0.02087	-0.01316
0.03409	-0.01430
0.05050	-0.01460
0.07015	-0.01422
0.09292	-0.01329
0.11864	-0.01197
0.14712	-0.01034
0.17815	-0.00848
0.21150	-0.00645
0.24693	-0.00430
0.28417	-0.00210
0.32296	0.00011
0.36301	0.00232
0.40401	0.00450
0.44571	0.00669
0.48785	0.00893
0.53029	0.01117
0.57286	0.01327
0.61525	0.01504
0.65704	0.01635
0.69785	0.01721
0.73735	0.01760
0.77520	0.01751
0.81109	0.01695
0.84468	0.01592
0.87567	0.01447
0.90377	0.01265
0.92871	0.01056
0.95024	0.00828
0.96814	0.00591
0.98215	0.00361
0.99209	-0.00170
0.99803	0.00045
1.00000	0.00000